Check for updates

Strong forces in optomechanically actuated resonant mass sensor

JESPER HÅKANSSON,[1,2,*] BART KUYKEN,[1,2] AND DRIES VAN THOURHOUT[1,2]

[1]*Photonics Research Group, Ghent University & Imec, Belgium*
[2]*Center for Nano- and Biophotonics, Ghent University, Belgium*
[*]*jesper.hakansson@ugent.be*

Abstract: As resonance mass sensors shrink in order to improve the sensitivity, traditional methods of transduction and readout struggle to keep up with increasing resonance frequencies and decreasing feature sizes. In this work we demonstrate an all-photonically transduced resonant mass sensor that manages to deal with these problems. The strong optomechanical force in slot waveguides is used to drive the mechanical resonanator giving a good signal to noise ratio at low optical powers. Using 120 μW of modulated optical power we measure a frequency noise equivalent to being able to resolve 500 kDa.

References and links

1. P. Truitt, J. Hertzberg, C. C. Huang, K. Ekinci and K. Schwab, "Efficient and sensitive capacitive readout of nanomechanical resonator arrays," Nano Lett. **7**(1), 120–126 (2007).
2. M. H. Bao, H. Yang, H. Yin and S. G. Shen,"Effects of electrostatic forces generated by the driving signal on capacitive sensing devices," Sensors Actuat. A: Phys. **84**(3), 213–219 (2000).
3. M. Li, W. H. P. Pernice and H. X. Tang, "Broadband all-photonic transduction of nanocantilevers," Nat. Nanotechnol. **4**(6), 377–382 (2009).
4. K. Zinoviev, C. Dominguez, J. A. Plaza, V. J. C. Busto, L.M. Lechuga, "A novel optical waveguide microcantilever sensor for the detection of nanomechanical forces," Journal of Lightwave Technology **24**(5), 2132–2138 (2006).
5. D. Y. Fedyanin, Y. V. Stebunov, "All-nanophotonic NEMS biosensor on a chip," Sci. Rep. **5**, 10968 (2015).
6. L.B.Soldano and E.C.Pennings, "Optical multi-mode interference devices based on self-imaging: principles and applications," J. Lightwave Technol. **13**(4), 615–627 (1995).
7. Y. T. Yang, C. Callegari, X. L.Feng, K. L. Ekinci and M. L. Roukes, "Zeptogram-scale nanomechanical mass sensing," Nano Lett. **6**(4), 583–586 (2006).
8. D. Van Thourhout and J. Roels, "Optomechanical device actuation through the optical gradient force," Nat. Photonics **4**(4), 211–217 (2010).
9. V. R. Almeida, Q. Xu and C. A. Barrios and M. Lipson, "Guiding and confining light in void nanostructure," Opt. Lett. **29**(11), 1209–1211 (2004).
10. P. T. Rakich, M. A. Popovic and Z. Wang, "General treatment of optical forces and potentials in mechanically variable photonic systems," Opt. Express **17**(20), 18116–18135 (2009).
11. R. Van Laer and B. Kuyken and D. Van Thourhout and R. Baets, "Analysis of enhanced stimulated Brillouin scattering in silicon slot waveguides," Opt. Lett. **39**(5), 1242–1245 (2014).
12. N. Kacem and J. Arcamone and F. Perez-Murano and S. Hentz, "Dynamic range enhancement of nonlinear nanomechanical resonant cantilevers for highly sensitive NEMS gas/mass sensor applications," J. Micromech. Microeng. **20**(4), 045023 (2010).
13. T. Spuesens and S. Pathak and M. Vanslembrouck and P. Dumon and W. Bogaerts, "Grating Couplers With an Integrated Power Splitter for High-Intensity Optical Power Distribution," IEEE Photon. Technol. Lett. **28**(11), 1173–1176 (2016).
14. M. Pruessner, N. Siwak, K. Amarnath, S. Kanakaraju, WH. Chuang and R. Ghods, "End-coupled optical waveguide MEMS devices in the indium phosphide material system," J. Micromech. Microeng. **16**(4), 832 (2006).
15. G. Anetsberger, R. Riviere A. Schliesser, O. Arcizet and T. Kippenberg, "Ultralow-dissipation optomechanical resonators on a chip," Nat. Photonics **2**(10), 627–633 (2008).
16. K. L. Ekinci, Y. T. Yang and M. L. Roukes, "Ultimate limits to inertial mass sensing based upon nanoelectromechanical systems," J. Appl. Phys. **94**(5), 2682–2689 (2004).
17. D. Taillaert, W. Bogaerts, P. Bienstman, T. F. Krauss, P. Van Daele, I. Moerman, S. Verstuyft, K. De Mesel and R. Baets, "An out-of-plane grating coupler for efficient butt-coupling between compact planar waveguides and single-mode fibers," IEEE J. Quantum Electron. **38**(7), 949–955 (2002).

18. E. Forsen, G. Abadal, S. Ghatnekar-Nilsson, J. Teva, J. Verd, R. Sandberg, W. Svendsen, F. Perez-Murano, J. Esteve, E. Figueras, F. Campabadal, "Ultrasensitive mass sensor fully integrated with complementary metal-oxide-semiconductor circuitry," Appl. Phys. Lett. **87**(4), 043507 (2005).

19. G. Vidal-Álvarez, J. Agustí, F. Torres, G. Abadal, N. Barniol, J. Llobet, M. Sansa, M. Fernández-Regúlez, F. Pérez-Murano, Á. San Paulo and O. Gottlieb, " Top-down silicon microcantilever with coupled bottom-up silicon nanowire for enhanced mass resolution," Nanotechnology **26**(14), 145502 (2015).

Over the last few years rapid advances in mass sensing have been made exploiting the progress in micro- and nano-fabrication of mechanical resonators to reach new levels of sensitivity. By measuring the shift in resonance frequency when a small sample mass (e.g. a protein molecule) is attached to a resonator it is possible to calculate the added mass. The resonance shift increases as the resonator is reduced in mass, this comes with the price of increasing the difficulty in detecting and driving the increasingly small nanomechanical resonators.

Out-of-plane interferometric displacement detection has problems resolving features below the Rayleigh limit and capacitive readout schemes suffer as the capacitance decreases with the size of the resonator [1]. A bias voltage can be used to offset the problem of decreasing capacitance but comes at the risk of electrical pull-in [2] . These problems could be alleviated with an integrated photonic approach and would lead to a cost reduction of the sensor. During the last few years a few optically actuated MEMS resonators integrated in a photonics waveguide platform have already been demonstrated [3–5]. These devices offer the possibility of using cheap and widely available telecom lasers and photodetectors and are fabricated using cost-effective wafer scale processes.
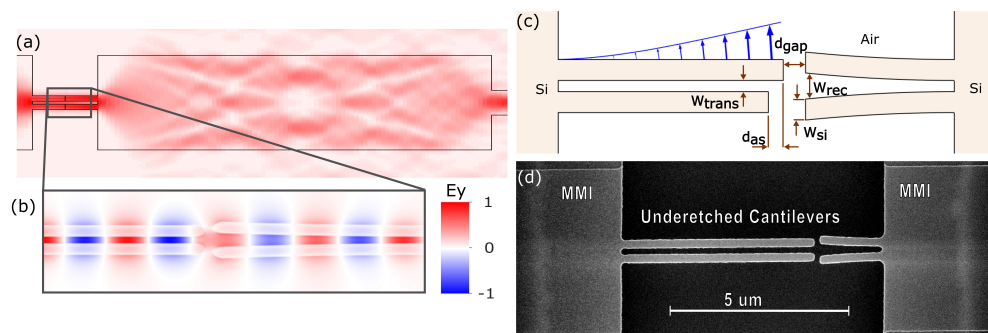

Fig. 1. (a) The optical field envelope, red, in the MMI, black outline. (b) The normalized Ey field in the slot. The field concentration in the slot and at the edges of the waveguide outlines the structure. (c) A schematic drawing of the SWG section of the device. The blue arrows and line are proportional to the displacement of the first order mechanical mode shape. (d) SEM image of the transmitting SWG, on the left side, and the widened receiving SWG, on the right side. Both are underetched.

In this work we demonstrate the first cantilever sensor making use of the strong actuation force found in slot waveguides (SWG) [8]. In the device, Fig. 1, the SWG is end-coupled to another SWG thus forming a system of in total four cantilevers. If any of the cantilevers moves the transmission through the device will be affected, resulting in a direct readout of the vibrations. The strong optomechanical transduction offers a way to generate a strong driving force at low optical powers and a high signal to noise ratio. Another benefit is that the forces between the cantilevers forming the SWG act in the plane of the lithography. This means that it is possible to optimize the vibrational mode and readout in the design phase. This is different when relying on out of plane vibrations, in which case it is more difficult to control the transduction [3]. The SWGs are anchored in a multimode interferometer (MMI) making it possible to transition directly

to a waveguide from a much wider block of silicon [6]. This anchoring offers a stark contrast in mechanical stiffness to the flexible cantilever, resulting in a high mechanical quality factor. The design fabricated that gave the best coupling to the SWG is a 48.4 μm long by 11 μm wide between two trenches etched 70 nm deep. In the current case the MMI was designed as a 1-to-1 mirroring device but it is also possible to use 1-to-N devices, multiplexing several cantilevers similar to what was shown in [3]. To introduce the test mass one could use a gas nozzle and then track the mass induced frequency shift with a phase locked loop, PLL, similar to what is used in [7]. In this case a PLL locks on to the phase of the resonator. By tuning the PLL to lock to the resonator phase response at resonance and then tracking the PLL signal to the voltage controlled oscillator it is possible to record the change in resonance frequency.

The mechanical vibrations are imprinted on the optical signal by their perturbation of the mode coupling over the gap between the two SWG, [14]. The transmission can be described by,

$$T_{tra} = |\int_{-\infty}^{\infty} F(\phi_{input}(x, y, z), d_{gap})\phi_{output}(x, y, z)dxdy|^2 \qquad (1)$$

whereby $\phi_{input,output}$ are the optical modes in the facing waveguides and the function F describes how the mode diverges over the gap, d_{gap}. The divergence of the light in the free space coupling gap is dependent on the dimensions of the SWG and particularly the width of the slot at the ends of the coupling section [14]. Simulations using Lumerical FDTD show that the sensitivity, $\epsilon_{om} = \delta T_{tra}/\delta U$ increases for a decreasing gap d_{gap} which therefore is chosen to be 100 nm, the minimal width that can be fabricated in our process (U is the displacement at the tip of the cantilever). Figure 2(d) shows how the displacement sensitivity changes with the width of the sensing slot W_{trans} and the width of the facing slot W_{rec} respectively. The width of the silicon cantilevers W_{si} was set at W_{si}=280 nm for which simulations show the optomechanical force in the SWG is maximized, Fig 2(b). The figures show that it is possible to enhance the displacement sensitivity by choosing different widths for the transmitting and receiving slot. Again, taking into account the technological limits of the process, we defined W_{trans} = 100 nm, W_{rec} = 280 nm. A fabricated sample can be seen in Fig. 1(d). For this configuration the sensitivity is simulated to be $\epsilon_{om} = 1.2\mu m^{-1}$.

It has been shown that light propagating in a SWG can generate a strong attracting optomechanical force between the two cantilevers [8]. This is because the effective refractive index of the optical mode has a strong dependency on the slot width [9]. The attractive force can then be calculated [10, 11],

$$F = \frac{P_{op}L}{c}\frac{dn_{eff}}{du} \qquad (2)$$

where L is the length of the cantilever, dn_{eff}/du the change in effective refractive index per displacement, c the speed of light and P_{op} the optical power in the waveguide. Simulations show that for a wider slot the refractive index is exponentially dependent on the slot width. When the slot is narrower, the second beam can no longer be treated as a perturbation of the field around the first beam [9]. In that case the force dependence on slot width, seen in Fig. 2(a), show a very good correspondence to the inverse of a second order polynomial. Fitting a curve to the force calculated from a simulation of the effective refractive index then gives $p_{fit}(w) = P_{op}L/(6.72 + 7.37 \cdot 10^8 w + 5.29 \cdot 10^{15} w^2)$, where w is the slot width. Because of the inverse square dependence of the force with respect to the slot width, the drive induced nonlinearities can be treated similarly to how they were treated in capacitively driven MEMS devices before [12]. Using this method it is possible to calculate the critical amplitude, the amplitude limit where exceeding it the resonator is bistable. Using this method it is possible to calculate the critical amplitude, the amplitude limit where exceeding it the resonator is bistable. The bistability occurs mainly due to the optomechanical nonlinearity shifting the resonance
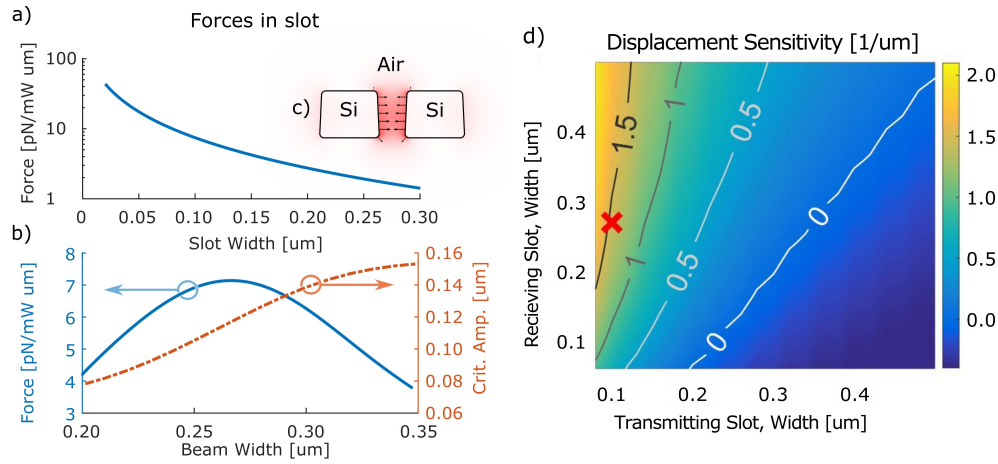
Fig. 2. (a) The attractive force in the slot waveguide, assuming 280 nm beam width. (b) Critical amplitude and force acting on the SWG as a function of cantilever width. The critical amplitude is calculated assuming a 1 mW CW optical power in the waveguide and a 100 nm slot width. (c) The optical mode, $|E|^2$ in red, and the force distribution on the edge of the waveguide, black arrows. Side walls slanted in accordance with XSEM of fabricated cantilevers.(d) A map of the displacement sensitivity as relative to the incoming power, for vibrations in the transmitting slot detected with a 1550 nm laser probe. The displacement sensitivity of a slot cantilever is dependent on the vibrating slot's width as well as the width of the opposite slot. The red cross marks the vibration sensitivity of the fabricated design. This is for cantilevers of equal length.

frequency of the resonator as the amplitude increases. In order to avoid nonlinear effects it is important for the amplitude to stay well below critical amplitude. It can be written as

$$u_{crit} = \frac{4\sqrt{2}}{3\sqrt{-\sqrt{3}(P_{CW}p_3\Psi_3 + k_3)/\omega_0\Gamma m_{eff} - p_2\Psi_2/p_0\Psi_0}} \tag{3}$$

where $\Psi_n = 1/L \int_0^L \psi(s)^{n+1}ds$ is a lumped parameter for how the mechanical mode, ψ, interacts with the n-th order Taylor expansion coefficient, p_n, of the force. P_{CW}, ω_0, m_{eff} and Γ are the average optical power in the SWG, the mechanical resonance frequency, the effective mass and the loss rate. k_3 is the third order nonlinearity of the stiffness inherent to the cantilever shape [12]. The critical amplitude is reached with a modulated optical power of, $P_{mod,crit} = 4u_{crit}\omega_0\Gamma/(4p_0\Psi_0 + p_2\Psi_2 u_{crit}^2)$, assuming it does not exceed the slot width, see Fig. 2(b).

In a resonant mass sensor, as a particle is absorbed by the cantilever, the mass of the resonator increases. The change of mass results in a decrease of the mechanical resonance frequency. Assuming the cantilever can be considered as a harmonic oscillator the responsivity to a small added mass, $\delta m \ll m_{eff}$, is $R \approx -\omega_0/(2m_{eff})$. The vibrations of a cantilever are well described by classical beam theory. With beam theory we can calculate the effective mass from the resting mass, $m_{eff} = \Psi_1 m_{rest}$.

The resonator model is complicated slightly by the short distance between the anchoring points of the two silicon cantilevers of the SWG. Because of their proximity it is inevitable that they exhibit a mechanical coupling introducing a small perturbative effect on the resonance frequency. This splitting can be described with [15],

$$\omega_{\pm} = \frac{\omega_1 + \omega_2}{2} + i\frac{\Gamma_1 + \Gamma_2}{4} \pm \sqrt{(\frac{\omega_1 - \omega_2}{2} + i\frac{\Gamma_1 - \Gamma_2}{4})^2 + \frac{g^4}{4\omega_1\omega_2}} \tag{4}$$

where $\omega_{\pm}$ are the complex frequencies of the supermodes, $\omega_{1,2}$ and $\Gamma_{1,2}$ are the resonance frequencies and loss rates of the individual cantilevers and g is the coupling coefficient. From this equation it can be seen that if the coupling $g^2/(\omega_1\omega_2)^{1/2}$ is small in comparison to the individual frequency splitting of the two cantilevers the coupling can be ignored in terms of its effect on the mass responsivity. Therefore we have chosen to shorten one of the two cantilevers deliberately by 100 nm, d_{as}, in order to detune them. This corresponds to a measured change of the resonance frequency by 440 kHz for a 6 μm cantilever as compared to the measured 38 kHz coupling induced splitting measured in a pair designed to be identical in length. The reduction in length comes at the cost of -0.2 dB of displacement sensitivity. It is possible to detune the cantilevers further by either making one cantilever thinner or by shortening it further.

The smallest frequency change that can be determined is dependent on the mechanical frequency noise. The fundamental noise source is expected to be thermomechanical. From the equipartition theorem it is possible to calculate the thermomechanical noise amplitude [16],

$$S_{xx}^{1/2} = \sqrt{\frac{4k_bTQ_{mech}}{\omega_0^3 m_{eff}}} \tag{5}$$

where k_b is Boltzmann's constant, T is the cantilever temperature and Q_{mech} is the mechanical quality factor. Compared to the thermomechanical noise, the direct optomechanical noise force should not be a problem as the mechanical frequency noise caused by intensity noise of even a cheap laser is several orders lower than the thermomechanical frequency noise, at our optical powers [5]. The pump also imprints directly on the probe via direct optical nonlinearities such as the Kerr effect and two photon absorption. The Kerr effect should be negligible as the device is broadband and two photon absorption for a device of this length and for the powers used is smaller than the mechanically induced optical modulation by two orders of magnitude [13].

The smallest mass we can measure assuming that the thermomechanical noise is dominating the measurement can be calculated from the resulting frequency noise and mass responsivity [16],

$$\delta m = \frac{1}{R}\sqrt{\frac{E_{th}}{E_c}}\sqrt{\frac{\Delta_f\omega_0}{Q_{mech}}} = \sqrt{\frac{4\Delta_f k_b T m_{eff}^3 \omega_0}{Q_{mech}^3 F^2}} \tag{6}$$

where Δ_f is the measurement bandwidth, $E_c = m_{eff}\omega_0^2 U^2/2$ is the maximum drive energy, $E_{th} = k_bT/2$ is the thermal energy. Taking into account the length dependency of the force, mass and frequency we find that $\delta m \propto L^{-1/2}$. Hence, to reach a higher mass sensitivity it seems beneficial to increase the length of the cantilevers. However, this is only possible to a limited extent: the high optomechanical force in the SWG results in a high vibration amplitude for the longer cantilevers, inducing non-linearities and eventually collapsing the slot. The dependence of the mass sensitivity on the silicon cantilever width is more complicated as the dependence is nonlinear, see Fig. 2(b).

The fabrication of the mass sensor has been kept as simple as possible. It was patterned in a 220 nm thick silicon layer on top a 2 μm silicon oxide(SOI) using 193 nm UV lithography (www.ePIXfab.eu) after which the cantilevers were freed from the substrate with buffered hydrofluoric acid (1:7 $NH_4F : HF$). In order to avoid stiction for the longer cantilevers, >4 μm , this is followed by a critical point drying step. We couple in and out of the chip vertically using fiber grating couplers [17], losing 5.5 dB at each instance. Insertion loss of the device accounts for the remaining 3 dB that is lost over the device. The device as well as the fibers used for coupling in and out of the chip are placed in a vacuum chamber evacuated below 10^{-2} mbar for

each measurement. The thermomechanical noise is measured at 1563 nm with a transmission measurement using a high speed photo diode connected to an electric spectrum analyzer (ESA). The results can be seen in Fig. 3(a). The two cantilevers are 6 and 5.9 μm long, have a resonance frequency of 9.56 and 10.0 MHz and a quality factor of 4500 and 4600. For the 6 μm cantilever the effective mass is 215 fg and the mass responsivity 146 ZHz/kg. Details of the setup can be found in the method section.

It is possible to derive the displacement sensitivity from the measured displacement noise [3]. Comparing the calculated displacement noise, Eq. (5), with a measurement of the transmission noise makes it possible to extract the displacement sensitivity experimentally. Since it is possible to directly measure the eigenfrequency and quality factor, the uncertainty in the calculated thermomechanical noise is in the exact temperature of the cantilever. The thermomechanical noise of the 6 μm cantilever, the most sensitive of the cantilevers we fabricated, is measured to be -116 dBc/Hz if normalized to the carrier. Figure 4(b) shows the displacement sensitivity measured over a wavelength span of 30 nm. The measured values compare well with the simulated value. Figure 4(a) shows the measured mechanical frequency of several cantilever lengths, comparing well to the the inverse square dependency predicted by beam theory.
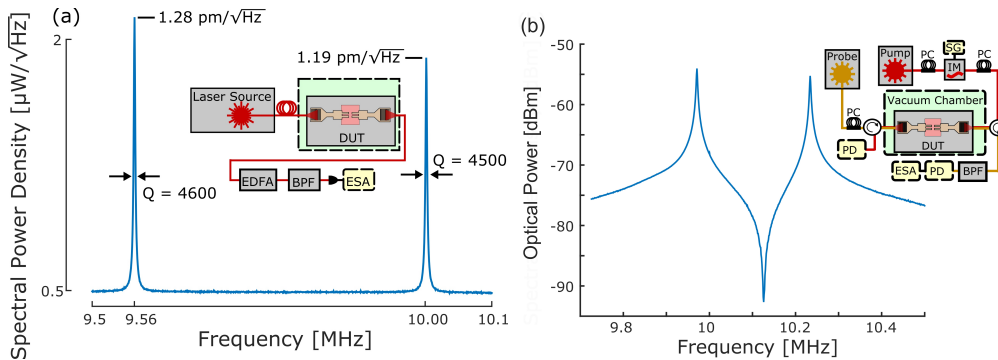

Fig. 3. (a) A transmission measurement of the thermomechanical vibrations of 6 and 5.9 μm long, 280 nm wide and 220 nm thick cantilevers. The carrier power impinging on the diode has been amplified with an EDFA to 1 mW. The noise amplitudes expected at room temperature is marked next to the corresponding peak. (b) The modulation of the probe optical power while driven by the pump at the corresponding frequency. The pump laser passes through the intensity modulator (IM) that is driven by the signal generator (SG). The probe passes through the device (DUT) in the opposite direction and is then redirected away from the pump path by a circulator. The reflection of the pump is filtered out in the band pass filter (BPF) and detected by a photo diode. The signal from the diode is then processed by the electric spectrum analyzer (ESA).

Figure 3(b) shows the result of a driven experiment, combining a probe beam at 1555 nm with an intensity modulated pump, which excites the mechanical vibrations. The inset of the figure shows the details of the setup. The pump power leaving the chip is 60 μW, which corresponds to 120μW of modulated intensity in the cantilevers. After the light couples out of the chip the pump is filtered out and the probe power read by the photo diode. To balance the extinction of the pump after the filter with the power coupled through the grating coupler the pump wavelength is offset from the probe wavelength by 15 nm to 1570 nm.

Figure 4(c) shows a direct phase noise measurement of the cantilevers taken with the ESA. The corresponding frequency noise gives for a 100 Hz measurement bandwidth a mass sensitivity of 500 kDa, 3 times more than Eq. (6) would suggest. We suspect that part of the extra noise at the lower frequency side of the noise spectrum is due to long term thermal drifts as there are no thermal stabilization in the vacuum chamber. The two peaks at 20 Hz and 100 Hz are
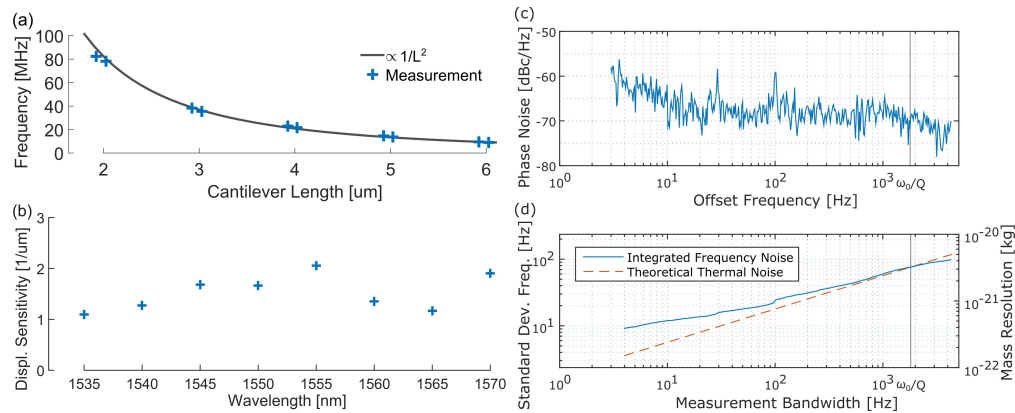
Fig. 4. (a) Measurements of a series of cantilevers of different length compared to the inverse square dependency on length expected from classic beam theory. (b) Shows the displacement sensitivity over a spectrum of wavelengths calculated from the amplitude of the thermal spectrum. The displacement sensitivity as relative to the power leaving the cantilevers. (c) Phase noise and (d) Frequency noise of a 6 μm cantilever. The calculated thermomechanical noise is included in the figure as a reference. Also marked is the mechanical decay rate ω_0/Q_{mech} marking the rate with which noise decays.

equipment related. Finally even though the cantilevers are separated in resonance frequency there are still a coupling between them that is not taken in to account for the analytical model of the noise. This mass sensitivity is in line with published sensors [18, 19] and previously suggested all-photonically transduced mass sensors [3, 5] while using a significantly smaller pump power. This makes it possible to limit imprint via material nonlinearities from the the pump onto the probe. The mass sensitivity should be possible to improve by increasing optical pump power and mechanical quality factor. The optical pump power is for the current setup limited by the tolerances of the modulator. Initial tests show that the mechanical quality factor improves with the removal of surface oxide, improvements that are then lost again as the oxide regrows.

The shorter cantilevers have a shorter optomechanical interaction length and as such they have a less efficient transduction. Because of this, even if the effective mass decreases, the signal to noise ratio decreases and the mass sensitivity is slightly worse for a given pump power.

The coupling between the two cantilevers that makes the SWG is possible to modify by changing the anchoring into the MMI. This should allow for minimizing the noise coupled between the resonators or move to a coupled resonator mass sensing scheme.

We have demonstrated an all-photonically transduced, CMOS compatible resonant mass sensor in the SOI platform. Exploiting the strong gradient force in slot waveguides to actuate the vibrations results in a strong signal to noise ratio with respect to the thermomechanical noise. Relying on in-plane vibrations makes it possible to optimize the displacement sensitivity and mechanical mode shape in the design phase. Using 120 μW of modulated optical power the sensors fabricated are measured to be able to resolve 500 kDa.

Methods The measurements have been performed with a Syntune S7500 tunable laser as the probe, a Santec TSL 510 tunable laser as the pump, an HP Lightwave 70810B high-speed photodiode and a Keysight N9010A EXA Signal Analyzer. The EDFA used is of type Keopsys CEFA-C-HG.